Neuroscience 274 (2014) 318–330

TARGETING THE MOTOR END PLATES IN THE MOUSE HINDLIMB GIVES ACCESS TO A GREATER NUMBER OF SPINAL CORD MOTOR NEURONS: AN APPROACH TO MAXIMIZE RETROGRADE TRANSPORT

R. MOHAN, A. P. TOSOLINI AND R. MORRIS *

Translational Neuroscience Facility, School of Medical Sciences, The University of New South Wales, Sydney, NSW, 2052, Australia

Abstract—Lower motor neuron dysfunction is one of the most debilitating neurological conditions and, as such, significantly impacts on the quality of life of affected individuals. Within the last decade, the engineering of mouse models of lower motor neuron diseases has facilitated the development of new therapeutic scenarios aimed at delaying or reversing the progression of these conditions. In this context, motor end plates (MEPs) are highly specialized regions on the skeletal musculature that offer minimally invasive access to the pre-synaptic nerve terminals, henceforth to the spinal cord motor neurons. Transgenic technologies can take advantage of the relationship between the MEP regions on the skeletal muscles and the corresponding motor neurons to shuttle therapeutic genes into specific compartments within the ventral horn of the spinal cord. The first aim of this neuroanatomical investigation was to map the details of the organization of the MEP zones for the main muscles of the mouse hindlimb. The hindlimb was selected for the present work, as it is currently a common target to challenge the efficacy of therapies aimed at alleviating neuromuscular dysfunction. This MEP map was then used to guide series of intramuscular injections of Fluoro-Gold (FG) along the muscles' MEP zones, therefore revealing the distribution of the motor neurons that supply them. Targeting the entire MEP regions with FG increased the somatic availability of the retrograde tracer and, consequently, gave rise to FG-positive motor neurons that are organized into rostro-caudal columns spanning more spinal cord segments than previously reported. The results of this investigation will have positive implications for future studies involving the somatic delivery and retrograde transport of therapeutic transgenes into affected motor neurons. These data will also provide a framework for transgenic technologies aiming at maintaining the integrity of the neuromuscular junction for the treatment of lower motor neuron dysfunctions.

Key words: Motor neurons, Motor end plates, Retrograde transport, Muscles, Fluoro-Gold, Mouse hindlimb.

*Corresponding author. Tel: +61-2-93858867.
E-mail address: renee.morris@unsw.edu.au (R. Morris).
Abbreviations: AChE, acetylcholinesterase; ALS, amyotrophic lateral sclerosis; FG, Fluoro-Gold; GDNF, Glial-derived Neurotrophic Factor; MEPs, motor end plates.

http://dx.doi.org/10.1016/j.neuroscience.2014.05.045

INTRODUCTION

Several neurological diseases can affect the control of movement and thus significantly impact on the quality of life of affected individuals. Such debilitating conditions include amyotrophic lateral sclerosis (ALS), spinal muscular atrophy and Duchenne muscular dystrophy. Throughout the recent years, the control of movement has received considerable attention from clinicians as well as scientists working on several models of these diseases in pre-clinical settings. In this regard, the last decade has seen the development of a large number of transgenic mouse models of neuromuscular dysfunctions (Hsieh-Li et al., 2000; Kaspar et al., 2003; Ishiyama et al., 2004; Turner et al., 2009; Wegorzewska et al., 2009; Kimura et al., 2010; Pratt et al., 2013). Such transgenic animal models are widely used to investigate the mechanisms underlying the development and progression of diseases affecting the control of movement and to develop therapeutic strategies aimed at delaying or reversing their progression. These strategies often involve the intramuscular targeting (and subsequent gene transfer to the corresponding spinal cord motor neuron) of viral vectors coding for therapeutic compounds such as neurotrophic factors (Acsadi et al., 2002; Kaspar et al., 2003; Azzouz et al., 2004; Nakajima et al. 2008; Wu et al. 2009; Benkhelifa-Ziyyat et al., 2013; for reviews see Gould and Oppenheim, 2011; Federici and Boulis, 2012). For instance, Acsadi and co-workers (2002) have demonstrated that intramuscular delivery of adenoviral vectors carrying the gene sequence for Glial-derived Neurotrophic Factor (GDNF) delays the onset of the disease symptoms in a transgenic mouse model of ALS. On the other hand, evidence obtained over the last years have revealed that degeneration of skeletal muscles and their neuromuscular junctions significantly contributes to the development and progression of ALS (for reviews see Kanning et al., 2010; Krakora et al., 2012). In mouse models of ALS, intramuscular delivery of GDNF to the muscle has proved to strengthen the neuromuscular junction (Suzuki et al., 2008) and delay the onset of the disease phenotype (Li et al., 2007).

Intramuscular delivery of therapeutic molecules therefore offers a promising approach for the treatment of neuromuscular disease as it has the potential to target both the muscles and the spinal cord motor neurons that supply them. However, the outcomes of pre-clinical trials involving muscle targeting for neuromuscular conditions have proved to

be sub-optimal in rescuing the disease phenotype arguably due, at least in part, to the limited protective capacity of these therapeutic compounds. A factor that could also significantly impede on the success of such therapies could be sub-optimal intramuscular delivery methods. Motor end plates (MEPs) are highly specialized regions of muscles that offer direct access to the pre-synaptic peripheral nerve terminals and, consequently, to the spinal cord motor neurons. It has been demonstrated that the efficacy of substance uptake is dependent upon the exact location of the injections, within the muscle, with regard to the motor end plate (MEP) region (Shaari and Sanders, 1993; Chin et al., 2005; Gracies et al. 2009; Van Campenhout and Molenaers, 2010). We have recently detailed the organization of the MEP zone for several forelimb muscles in the rat and mouse (Tosolini and Morris, 2012; Tosolini et al., 2013). In the diverse mouse models of neuromuscular dysfunction mentioned above, the hindlimb is often the target of investigation (Flood et al., 1999; Turner et al., 2009; Wegorzewska et al., 2009; Kimura et al., 2010; Henriques et al., 2011; Ngo et al., 2012; Pratt et al., 2013). The aim of the present investigation was therefore to characterize the muscle–motor neuron organization in the mouse hindlimb.

EXPERIMENTAL PROCEDURES

Subjects and housing

All experimental procedures complied with the Animal Care and Ethics Committee of the University of New South Wales and were performed in accordance with the National Health and Medical Research Council of Australia regulations for animal experimentation. The Animal Care and Ethics Committee of the University of New South Wales has approved the conduct of this study. A total of 34 naïve adult male C57BL/6 mice (Animal Resource Centre, WA, Australia) weighing between 20 and 30 g at the time of surgery were used in this study. The animals were housed in groups of 5 in an animal-holding room under a 12-h light–dark cycle. Food and water were provided *ad libitum* throughout the course of the experiment.

Acetylcholinesterase histochemistry

To minimize the use of animals, perfused mouse bodies ($n = 4$) were obtained through tissue sharing. Acetylcholinesterase histochemistry (AChE) was performed on these mouse carcasses as per Tosolini et al. (2013). The skin was removed from the carcasses and the entire bodies were immersed for 4 h at 4 °C in a solution containing 200 ml of phosphate buffer (PB), 290 mg of acetylthiocholine iodide, 600 mg of glycine, and 420 mg of copper sulfate (all reagents from Sigma–Aldrich, Castlehill, NSW, Australia). The carcasses were subsequently washed for 2 min in distilled water and developed by rapid immersion (i.e., 5–10 s) in a 10% ammonium sulfide solution.

Surgical procedures

Anesthesia was induced with isoflurane (Provet, Sydney, NSW, Australia; 1–2% in O_2). The fur covering the areas of interest was shaved and cleaned with 70% ethanol. For each muscle under investigation, a small incision was made in the skin to expose the muscle. Series of Fluoro-Gold (FG, 5% in distilled water; Fluorochrome, Denver, CO, USA) injections were manually performed through graded glass micropipettes (DKSH, Zurich, Switzerland) along the entire motor end plate (MEP) zone. The volume of FG varied between 2 and 4 µl depending on the size of the muscle. For example, Gluteus Maximus received four 1-µl injections of FG along its entire motor end plate region. Great care was taken to preserve the fasciae covering the targeted muscles as well as those surrounding it. Special care was also taken to ensure that the blood vessels surrounding the muscles were left intact. After the injections, the muscles were wiped with gauze to remove any tracer that may have inadvertently seeped from the injected muscle. A total of 43 series of intramuscular injections were performed into the following muscles: Gracilis ($n = 6$), Biceps Femoris ($n = 6$), Gluteus Maximus ($n = 4$), Vastus Medialis ($n = 8$), Semitendinosus ($n = 5$), Vastus Lateralis ($n = 6$), Gastrocnemius ($n = 4$) and Tibialis Anterior (n = 4). Gluteus Maximus was also targeted with either a 4-µl bolus injection of FG into the thickest part of the muscle ($n = 6$) or with 2-µl injections restricted to the antero-lateral or postero-medial portion of its MEP region ($n = 6$). In additional animals, 4 µl of FG was applied directly onto the intact fasciae covering Gluteus Maximus ($n = 4$). Moreover Gracilis, on which two distinct MEP zones are present, was targeted with 4 µl of FG or Fluorescein (Life Technologies Australia Pty., Mulgrave, Vic, Australia 3000 MW) either along the MEPs near the proximal ($n = 2$) or distal attachment ($n = 2$) of the muscle or along both MEP regions together ($n = 3$). One additional animal was also administered with a series of Fluoro-Gold injections along the entire MEP region of Gluteus Maximus to demonstrate the localization of the injections on a representative muscle. In all cases, the skin was subsequently closed with surgical clips (Texas Scientific Instruments LLC, Boerne, TX, USA) and the mice were monitored post-operatively until they recovered from the anesthesia.

Dissection and histology

After the intramuscular injections of FG, the mice were kept for 7 days to allow for optimal retrograde transport of the neuronal tracer. After this period of time, the mice received a lethal dose of Lethabarb (150 mg/kg; Virbac, Sydney, New South Wales, Australia) and were perfused intra-cardially with 0.1 M PB followed by 4% paraformaldehyde in 0.1 M PB. A midline incision was made along the gut of the perfused animals to remove the viscera and the muscles of the posterior abdominal wall and to identify the caudal-most rib, T13 and its adjoining vertebra (see Fig. 1A). The vertebra rostral to

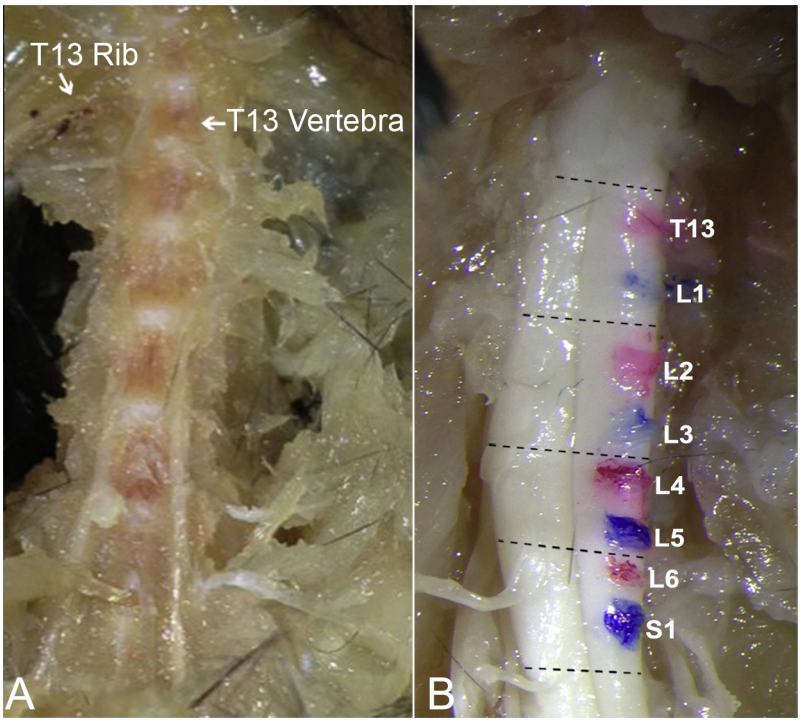

Fig. 1. Spinal cord segment dissection. (A) Ventral view of the spinal cord after the overlying muscles have been reflected and the abdominal viscera removed. The T13 ribs and vertebra are landmarks for the identification of the spinal root T13. (B) The exposed spinal cord with color markings that indicate the position of the ventral spinal roots (e.g., T13, L2, L4, and L6 in red; L1, L3, L5, and S1 in blue). The dashed lines indicate the locations where incisions were made to dissect out the two-segment blocks. (For interpretation of the references to color in this figure legend, the reader is referred to the web version of this article.)

T13 was subsequently removed to expose the T13 ventral root entry into the ventral horn of the spinal cord and this root was marked with red ink. The same procedure was carried out for each ventral root caudal to T13, and these were colored with markers of alternating colors to aid identification (i.e., T13, L2, L4 and L6 were colored in red whereas L1, L3, L5 and S1 were colored in blue) (see Fig. 1B). After this process, the exposed spinal cord was cut into two-segment blocks (i.e., T13–L1, L2–L3, L4–L5 and L6–S1 blocks). The upper and lower limits of each spinal cord segment were defined as the halfway points between two adjacent roots as they enter the cord. For each block of spinal cord tissue, a fiducial mark was made *in situ* in the white matter, half way between two adjacent roots to indicate the boundary between the segments. The two-segment blocks were then dissected out from the body, post-fixed overnight in a solution of 4% paraformaldehyde in 0.1 M PBS, after which they were cryo-protected in 30% sucrose (Sigma–Aldrich, Castle Hill, NSW, Australia) solution in distilled water for 3 days at 4 °C. Each block of spinal cord tissue was cut longitudinally into 50-μm-thick sections and mounted on microscope slides. The slides were air-dried overnight and were then cover-slipped with either an anti-fade medium containing DAPI (Invitrogen, Carisbad, CA, USA) or with Fluorescence mounting medium (Dako Australia Pty, Campbellfield, Vic, Australia).

Data analysis and presentation

After the AChE procedure, the hindlimbs were photographed, and Adobe Photoshop CS6 was used to transpose the locations of the MEPs onto a diagrammatic representation of the mouse hindlimb. The spinal cord tissue sections were photographed and analyzed under epifluorescence to detect the presence of FG- or Fluorescein-labeled motor neurons. Motor neurons were considered positively labeled when fluorescent granulations were present within both the soma and at least one axon/dendrite (Vanderhorst and Holstege, 1997; Tosolini and Morris, 2012; Tosolini et al., 2013). Adjacent tissue was also scrutinized to eliminate double counting of motor neurons. For each tissue section, fluorescently labeled motor neurons were plotted as single black dots on a separate layer of a diagrammatic representation of the spinal cord using Adobe Photoshop CS6. Root exit points, the position of the central canal and the fiducial marks created during dissection were used as spatial references. The Adobe Photoshop layers were subsequently stacked together to create a single two-dimensional representation of the position of the motor neurons innervating each hindlimb muscle. For each muscle, individual data plots were then presented side by side on a schematic diagram of a spinal cord (Fig. 5). The data plots derived from intramuscular injections performed on the left hindlimb were transposed onto the right spinal cord to maintain consistency with the representation.

For each limb, the number of labeled motor neurons in each segment were counted and added to obtain the total number of labeled motor neurons in the pool (Table 1). For all muscles, data plots were then combined to form a representative motor neuron column and were presented concurrently in the rostro-caudal, dorso-ventral, and medio-lateral axes in the same figure (Fig. 8). Our criterion for including labeled neurons from Fig. 5 into Fig. 8 was that labeled neurons be present, in any particular segment, in a minimum of two data sets.

RESULTS

Motor end plate (MEP) localization

Overall, the location of the MEP region for each hindlimb muscle was conserved between animals. Fig. 2A, C shows the location of the MEP zones on the lateral and medial aspect of a mouse hindlimb, respectively. On these photographs, the boundaries of each muscle as well as the direction of their muscle fibers can be observed. The MEP regions appear as bands of darkly stained speckles that are positioned orthogonally with respect to the muscle fibers and span across the full width of the muscle. Fig. 2B, D shows the same hindlimbs, on which colors have been overlaid to help the identification of the eight muscles of interest: Gluteus Maximus, Semitendinosus, Biceps Femoris, Vastus Lateralis, Gastrocnemius, Vastus Medialis, Gracilis and Tibialis Anterior. On these overlays, dashed lines have indicated the positions of the MEP regions. For each muscle targeted, a single MEP region was observed. In the Gracilis muscle, however, two distinct MEP regions were seen across the muscle fibers, i.e., one proximal and one distal (see Fig. 2C, D).

The MEP zones for Gluteus Maximus and Semitendinosus are located mid-way along the muscle fibers. The MEP region for Biceps Femoris is located toward the distal end of the muscle, i.e. close to the knee joint. Biceps Femoris is comprised of three distinct heads: the anterior, posterior and accessory heads.

Table 1. Number of labeled motor neurons following intramuscular injections of Fluoro-Gold into each muscle. The numbering of the data sets (1–6) in the table follows that of the motor columns (from left to right) in Fig. 5

Muscle	Dataset 1	Dataset 2	Dataset 3	Dataset 4	Dataset 5	Dataset 6
Gracilis	223	123	137	164		
Biceps Femoris	264	281	238	188		
Gluteus Maximus	216	216	273	304		
Vastus Medialis	102	131	146	163		
Semitendinosus	41	126	100	82	52	
Vastus Lateralis	49	53	51	59	54	90
Gastrocnemius	60	43	62	45		
Tibialis Anterior	114	86	107	177		

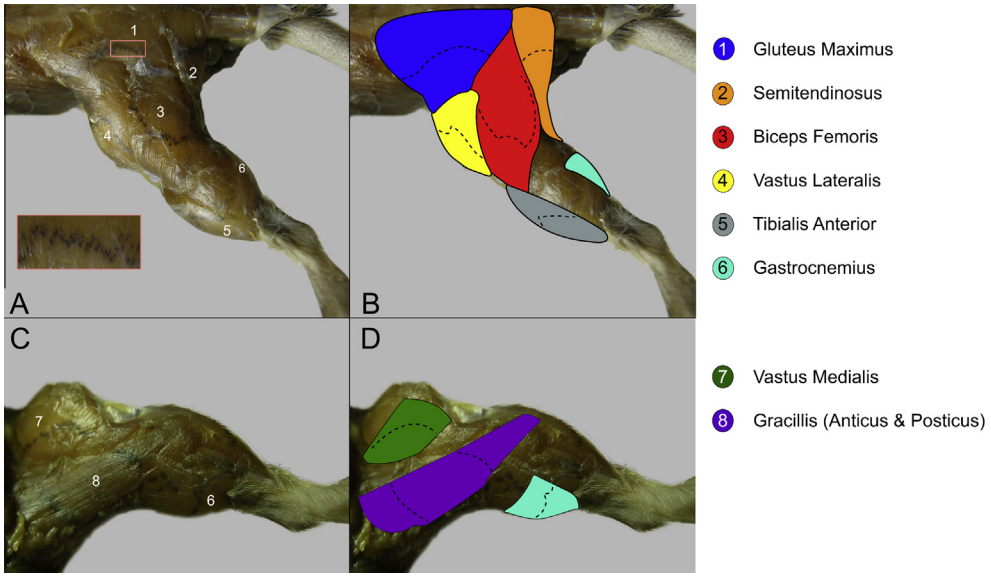

Fig. 2. Location of the motor end plate (MEP) zones on the mouse hindlimb. Lateral (A) and medial (C) superficial views of the mouse hindlimb following an acetylcholinesterase (AChE) histochemical reaction. The locations of the MEPs are indicated by the presence of black speckled lines that traverse the muscle fibers. The following muscles can be observed in (A): (1) Gluteus Maximus, (2) Semitendinosus, (3) Biceps Femoris, (4) Vastus Lateralis, (5) Tibialis Anterior, (6) Gastrocnemius. The inset in (A) is a close-up of the MEPs from Gluteus Maximus. In (C), the following muscles can be observed: (6) Gastrocnemius, (7) Vastus Medialis and (8) Gracilis. Lateral (B) and medial (D) superficial views of the same mouse hindlimb with color overlays that allow for easy identification of the targeted muscles. The dashed lines indicate the average location of the MEP zones based on acetylcholinesterase reactions of four hindlimbs.

However, despite this organization, the MEPs zone for Biceps Femoris spanned across all three heads in an almost continuous fashion. The MEP region for Vastus Lateralis and Vastus Medialis exhibit a skewed "S" shape across the muscle, spanning in a proximo-distal manner. Gracilis Anticus and Posticus have two MEP bands; one located in the proximal 1/5 of the muscle and the other is located in the distal 2/5 of the muscle. The MEPs for Tibialis Anterior exhibited an inverted "V" shape that spanned midway along the muscle. The MEPs on the Gastrocnemius muscle are linear in shape with a crest mid-way.

Localization of intramuscular injections into muscle

Fig. 3 pictures a typical muscle following intramuscular injections delivered into the MEP region. This figure illustrates that the spread of the FG tracer was restricted to the injected muscle only, without contaminating the neighboring muscles, as was the case for all series of injections.

Distribution of Fluoro-Gold-positive motor neurons innervating the mouse hindlimb

A total of 43 intramuscular injections of Fluoro-Gold were performed in the hindlimb. Eight of these injections produced weak and/or sparse labeling and are not mentioned henceforth. The remaining 35 injections produced intense retrograde labeling, and data from these injections have been included in the present analysis and are described later in the text. Fig. 4 illustrates a typical 50-μm-thick longitudinal section of the spinal cord to show the presence of fluorescently labeled motor neurons organized in a column. Motor neurons were defined as positively labeled if they displayed high levels of fluorescence in their cell body as well as in at least one process. Fig. 5 is a diagrammatic construct of the positively labeled neurons for each series of injections in the eight muscles of interest.

Gracilis. Gracilis Anticus and Gracilis Posticus run alongside each other on the medial aspect to adduct the hindlimb (Fig. 2C, D). Gracilis Anticus originates from the posterior half of the pubic symphysis and inserts into the medial border of the tibia. Gracilis Posticus originates from the ramus of the ischium and inserts into the tuberosity of the tibia. At the insertion point, Gracilis Anticus lies superficial to Gracilis Posticus (Greene, 1935). As they exhibit MEPs that are continuous with each other, the Gracilis muscles were targeted together. Six series of FG injections were performed on the Gracilis

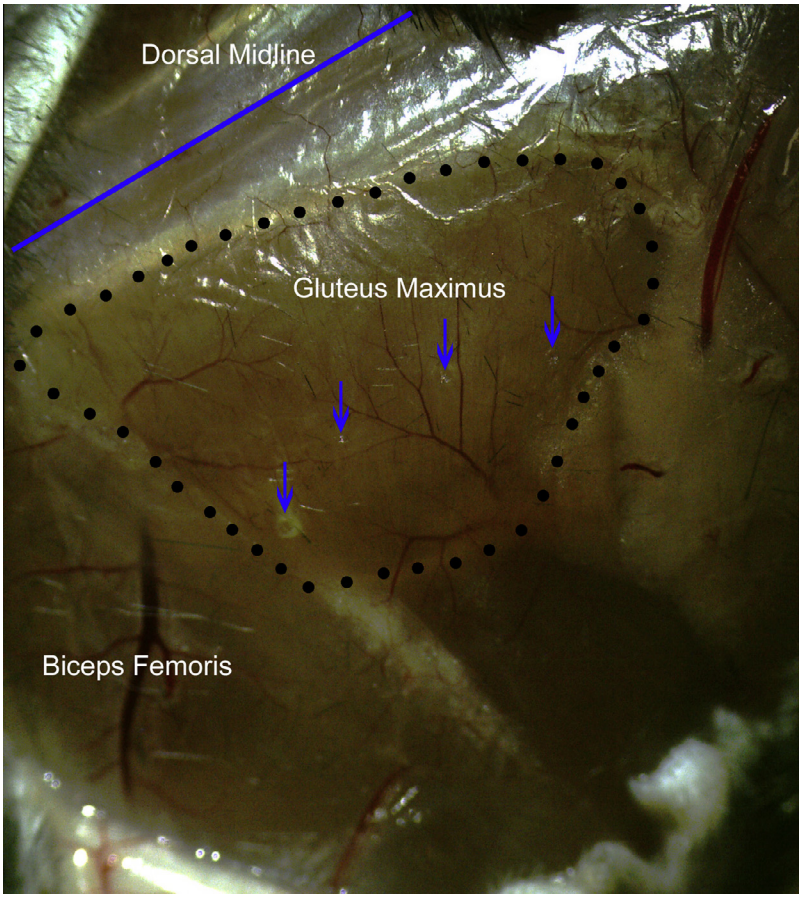

Fig. 3. Photomicrograph of Gluteus Maximus immediately after four injections of Fluoro-Gold along the MEP region. The border of the muscle is delineated with a series of black dots. The dorsal midline of the animal is indicated by a blue line. The location of the punctures left by the injections of the tracer is indicated by blue arrows. Note that the four injections are confined within the limits of the targeted muscle. (For interpretation of the references to color in this figure legend, the reader is referred to the web version of this article.)

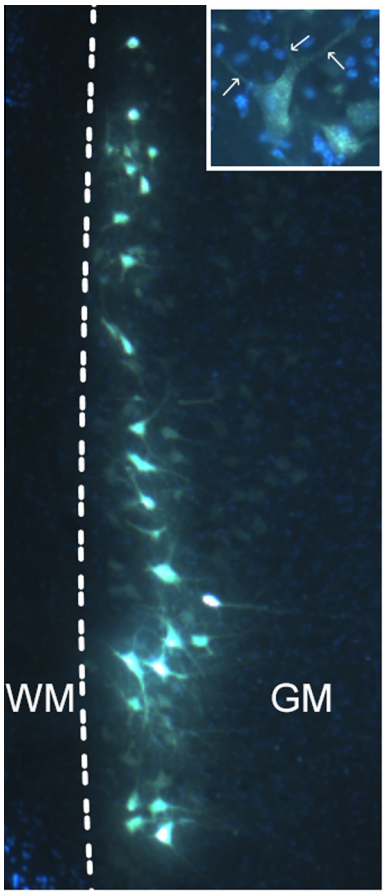

Fig. 4. Photomicrograph of a 50-μm-thick longitudinal section of a lumbar spinal cord demonstrating a typical column of Fluoro-Gold (FG)-labeled motor neurons counterstained with DAPI. The inset shows a labeled motor neuron at a higher magnification to show the FG granulations in the soma and processes. Arrows indicate dendritic processes extending from the cell body of a labeled neuron. The dashed line represents the border between the gray matter (GM) and the white matter (WM).

muscle, four of which were included in the analysis. Such injections gave rise to positively labeled motor neurons extending from L1 to the rostral part of L5 (Fig. 5A). In one series case, two labeled motor neurons were present in rostral T13. These two motor neurons were not taken into account in further analysis. The number of labeled motor neurons observed following the intramuscular injections into the Gracilis muscle was 223, 123, 137 and 164 for the included series of injections (Table 1).

Biceps Femoris. The Biceps Femoris muscle, which is a knee flexor, is located caudo-lateral to Gluteus Maximus and shares borders with Gluteus Maximus, Vastus Lateralis and Semitendinosus (Fig. 2A, B). In the mouse, Biceps Femoris has three heads, instead of the two present in humans. The anterior head has its origin in the last sacral vertebra and the coccyx. Both the accessory and posterior heads arise from the sciatic tuber. The Biceps Femoris muscle inserts into the distal end of the femur (Greene, 1935). Biceps Femoris was targeted with six series of FG injections, of which four were included in the analysis (Fig. 5B). These injections resulted in positively labeled motor neurons spanning from T13 to rostral S1. The number of labeled motor neurons observed following the intramuscular injections into the Biceps Femoris muscle was 264, 281, 238 and 188 for the included series of injections (Table 1).

Gluteus Maximus. The Gluteus Maximus muscle, a muscle that extends the hip, is located on the lateral aspect of the mouse hindlimb (Fig. 2A, B). It is the most superficial of the Gluteal muscles and overlays Gluteus Medius. It has its point of origin in the dorsal border of the ilium and inserts into the third trochanter of the femur (Greene, 1935). On its anterior border, it joins with the Tensor Fasciae Latae muscle, and its posterior aspect is covered by the anterior head of Biceps Femoris. Four series of FG injections were performed into Gluteus Maximus and all of them resulted in intense labeling in the ventral horn of the spinal cord, between spinal cord segments L2 and S1 (Fig. 5C). The number of labeled motor neurons observed following the intramuscular injections into the Gluteus Maximus muscle was 216, 216, 273 and 304 for the included series of injections (Table 1).

Vastus Medialis. Vastus Medialis is the most medial of the quadriceps femoris muscles that extend the knee. It has its origin in the neck and proximal end of the shaft of the femur and has its insertion into the tibial tuberosity via the patella ligament (Greene, 1935). It is bounded by the Rectus Femoris, laterally and Adductor Magnus, medially (Fig. 2C, D). Vastus medialis was targeted with eight series of FG injections, four of which were included in the analysis. As shown in Fig. 5D, these series of injections gave rise to FG-positive motor neurons spanning from segments L1 to L3. In one series case, however, one labeled motor neuron was present in caudal T13 and this motor neuron was not taken into account in further analysis. The number of labeled motor neurons observed following the intramuscular injections into the Vastus Medialis muscle was 102, 131, 146 and 163 for the included series of injections (Table 1).

Semitendinosus. The Semitendinosus muscle is a knee flexor that originates on the lateral aspect of the hindlimb and inserts into the tuberosity of the tibia, distal to the Gracilis insertion (Greene, 1935) (Fig. 2A, B). Semitendinosus has two heads at its point of origin: the principal and the accessory heads. The principal head has its origin in the sciatic tuber whereas the accessory head originates from the last sacral and the following two coccygeal vertebrae. Semitendinosus was targeted with five series of FG injections and all five were included in the analysis. These injections resulted in labeled motor neurons extending from L4 to S1 (Fig. 5E). The number of labeled motor neurons observed following the intramuscular injections into the Semitendinosus muscle was 41, 126, 100, 82 and 52 for the included series of injections (Table 1).

Vastus Lateralis. Vastus Lateralis is the most lateral of the quadriceps muscles and is a knee extensor (Fig. 2A, B). It has its two points of origin in the greater trochanter

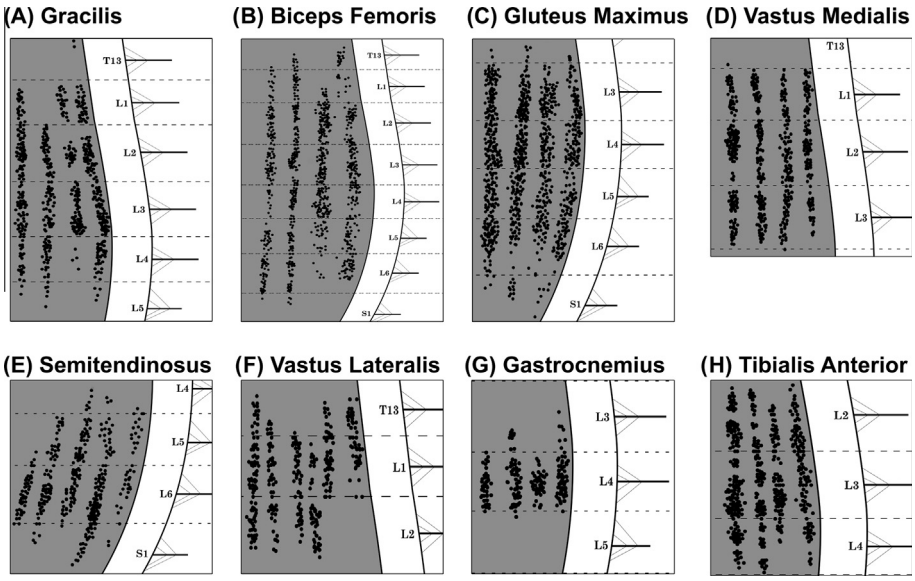

Fig. 5. Composite diagram illustrating the distribution of labeled motor neurons from individual intramuscular injections. In A–H, each dot represents one labeled motor neuron and each column of motor neurons represents the results from one series of intramuscular injections of Fluoro-Gold. The dashed lines in each diagram represent the half-way point between adjacent nerve roots.

and the third trochanter of the femur and it inserts into the tuberosity of the patella via the patella ligament (Greene, 1935). Anteriorly, it shares a border with the Tensor Fasciae Latae muscle as well as with Gluteus Maximus. Vastus Lateralis is located medial to the anterior head of Biceps Femoris and lateral to Rectus Femoris on the medial aspect of the hindlimb. Vastus Lateralis was targeted with six series of FG injections, all of which were included in the analysis. Such injections gave rise to labeled motor neurons extending from segments T13 to L2 (see Fig. 4F). The number of labeled motor neurons observed following the intramuscular injections into the Vastus Lateralis muscle was 49, 53, 51, 59, 54 and 90 for the included series of injections (Table 1).

Gastrocnemius. The Gastrocnemius muscle is located on the posterior, distal end of the hindlimb and plantar flexes the ankle joint (Fig. 2A–D). Proximally, Gastrocnemius has a medial and a lateral head. The medial head has its origin in the medial epicondyle of the femur and the medial fabella. The lateral head originates from the lateral epicondyle of the femur and the lateral fabella (Greene, 1935). Distally, Gastrocnemius joins the Soleus muscle to form the calcaneal tendon, which inserts into the tuber calcanei. Gastrocnemius was targeted with four series of FG injections, all of which were included in the analysis. These injections resulted in positively labeled motor neurons extending across spinal segments L3 and L4 (Fig. 5G). In one series case, however, one labeled motor neuron was present in rostral L5 and was not taken into account in further analysis. The number of labeled motor neurons observed following the intramuscular injections into the Gastrocnemius muscle was 60, 43, 62 and 45 for the included series of injections (Table 1).

Tibialis Anterior. Tibialis Anterior is one of the most prominent dorsiflexor muscles located in the anterior compartment of the lower hindlimb (Fig. 2A, B). It originates from the lateral condyle of the tibia, and its distal tendon crosses over to the medial aspect of the limb and inserts into the first cuneiform and the first metatarsal (Greene, 1935). The Tibialis Anterior muscle was targeted by four series of FG injections, all of which were included in the analysis. These injections produced labeled motor neurons extending from L2 to L4 (Fig. 5H). The number of labeled motor neurons observed following the intramuscular injections into the Tibialis Anterior muscle was 114, 86, 107 and 177 for the included series of injections (Table 1).

Fluoro-Gold injections to sub-regions of the MEP zone for Gluteus Maximus

Fig. 6A is a schematic representation of the sub-regions of the MEP zone of Gluteus Maximus that were selectively targeted with FG. These sub-regions are the antero-lateral (n = 3) and the postero-medial (n = 3) halves as well as the center of the MEP zone (n = 4). Additionally, but not shown in this figure, FG was applied (i.e., not injected) directly onto the fascia covering Gluteus Maximus (n = 4). Fig. 6B shows the distribution of the FG-labeled motor neurons resulting from the above-described injections. In this figure, one of the columns of motor neurons obtained from the delivery of FG along the full length of the MEP region for Gluteus Maximus (see Fig. 5C) was added for comparison purposes. FG injections along the entire MEP region in Gluteus Maximus resulted in labeling between spinal cord segments L2 and S1. In contrast, bolus injections of FG in the center of the MEP zone resulted in the labeling of motor neurons limited to segments L4–L6. Moreover, FG injections confined to the antero-lateral and postero-medial aspects of the MEP zone for Gluteus Maximus gave rise to labeled motor neurons extending from segments L5 to S1 and

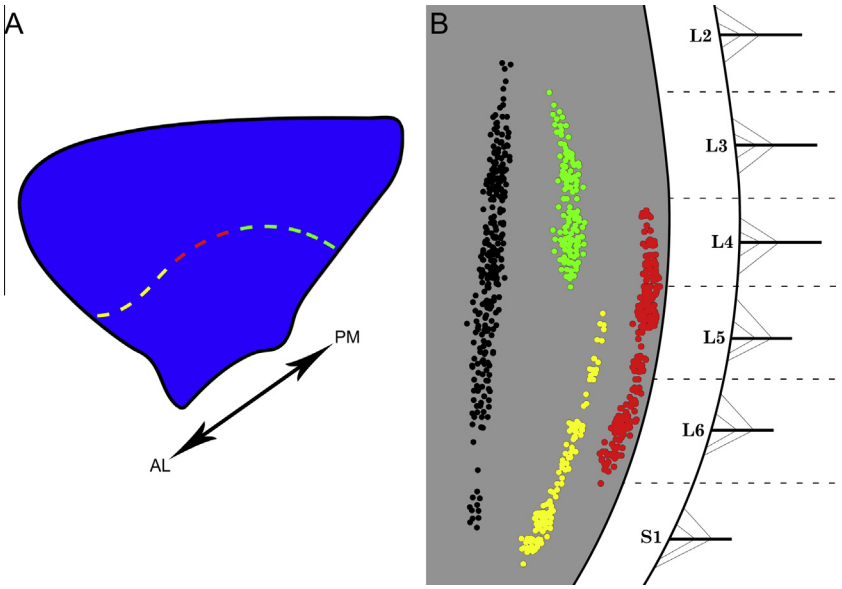

Fig. 6. Selective targeting of subregions of the motor end plate zone in Gluteus Maximus and the resulting labeling in the corresponding spinal cord motor neurons. (A) Schematic representation of the subregions of the motor end plate (MEP) zones of Gluteus Maximus that were selectively targeted with Fluoro-Gold (FG). The yellow and green dashes represent the anterolateral and posteromedial subregions of the MEP zone, respectively. The red dashes represent the center of the MEP zone where a single bolus of FG was injected. (B) Distribution of the labeled motor neurons observed following the injections of FG into the subregions described in (A). In black is a column of labeled motor neurons resulting from injecting the entire span of the MEP zone in the Gluteus Maximus (taken from Fig. 4C). In green is a column of labeled motor neurons resulting from injections into the posteromedial subregion of the MEP zone. In yellow is a column of labeled motor neurons obtained after injecting the anterolateral section of the MEP zone. In red is a column of labeled motor neurons resulting from a bolus injection into the center of the MEP zone. The black dashed lines indicate the half-way points between adjacent spinal roots. AL: anterolateral; PM: posteromedial. (For interpretation of the references to colour in this figure legend, the reader is referred to the web version of this article.)

L3 to L4, respectively. Application of FG onto the intact fascia of the muscle did not produce any labeling (result not shown).

Retrograde tracer injections of Gracilis MEP bands

The Gracilis muscle exhibits two MEP bands, i.e., one proximal and one distal (see Fig. 2C, D). FG injections to each band individually or in combination gave rise to FG-labeled motor neuron columns of similar density located between segments L1 and L5 (data not shown). In another injection series, each MEP band was targeted with either FG or with Fluorescein, two neuronal tracers of different emission/excitation wavelength. For example, the proximal MEP band was injected with FG and the distal MEP band was injected with Fluorescein. This resulted in FG/Fluorescein double-labeled motor neurons (Fig. 7).

Organization of the motor neurons supplying the mouse hindlimb

Fig. 8 is a diagrammatic representation of the distribution of motor neurons for each muscle targeted in the present investigation. Motor neurons innervating the mouse hindlimb are organized into columns that span several segments of the spinal cord. Fig. 8A shows the distribution, on the rostro-caudal axis, of these columns. Together, these columns of motor neurons encompass segments T13–S1 of the mouse spinal cord, exhibiting a significant degree of overlap with each other. Fig. 8B illustrates that the overlap observed between the various motor neuron columns is not limited to the rostro-caudal axis but can also be observed in the transverse plane.

DISCUSSION

We have recently targeted the entire motor end plate (MEP) region of several muscles in the rat and the mouse forelimb with retrograde tracers (Tosolini and Morris, 2012; Tosolini et al., 2013). These tract-tracing analyses revealed that the motor neuron columns that supply forelimb muscles extend over more cervical spinal cord segments and display greater overlap with each other than previously reported. The aim of the present study was to characterize the muscle–motor neuron organization in the mouse hindlimb as it is often the target of therapeutic strategies aimed at alleviating dysfunction in engineered transgenic mouse models of neuromuscular disease (Flood et al., 1999; Turner et al., 2009; Wegorzewska et al., 2009; Kimura et al., 2010; Henriques et al., 2011; Pratt et al., 2013). A detailed map of the MEP zone for eight muscles of the mouse hindlimb was first produced. This map was then used to guide series of Fluoro-Gold (FG) injections throughout the entire MEP region of these muscles. Careful analysis of these series of retrograde tracer injections revealed the details of the topographical organization that exists between the different mouse hindlimb muscles and the columns of motor neurons that innervate them.

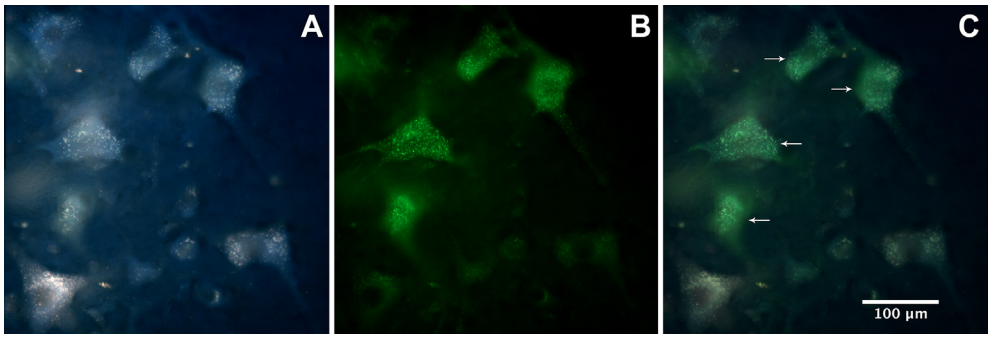

Fig. 7. Photomicrographs of labeled motor neurons following injections of Fluoro-Gold (FG) into the distal motor end plate (MEP) zone and Fluorescein into the proximal MEP zone of a single Gracilis muscle. (A) FG- and (B) fluorescein-labeled motor neurons resulting from this series of injections. (C) Overlay of panels A and B to show some double-labeled motor neurons indicated by arrows.

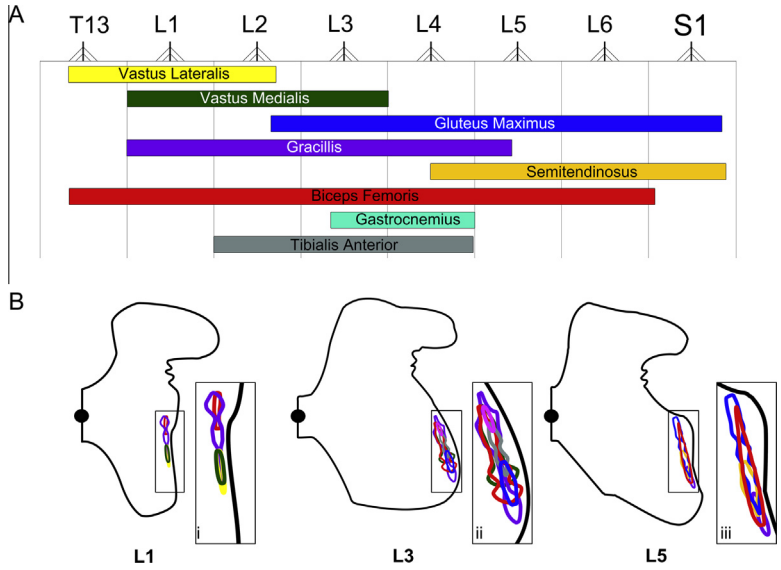

Fig. 8. Color-coded schematic maps of the motor neuron columns innervating the targeted hindlimb muscles. The color schemes remain consistent with that of Fig. 2B, D. (A) Rostro-caudal map of the motor neuron columns innervating the targeted hindlimb muscles. These columns were obtained by combining plots from Fig. 5. The nerve roots represent the halfway point between spinal cord segments throughout T13–S1. (B) Dorso-ventral and medio-lateral map of the motor neuron columns innervating the targeted hindlimb muscles for spinal cord segments L1, L3 and L5. The insets (i, ii and iii) represent magnification of the motor columns at these segments. The gray matter contours were adapted from Watson et al. (2009). (For interpretation of the references to colour in this figure legend, the reader is referred to the web version of this article.)

To our knowledge, the present study is the first characterization, by means of acetylcholinesterase (AChE) histochemistry, of the MEP distribution in the mouse hindlimb. This analysis revealed that the MEP zones of the hindlimb extend, in a continuous fashion, across the entire width of the muscles. In these muscles, the MEPs are located orthogonally to the direction of the muscle fibers but are seldom organized in a straight band. In muscles such as Vastus Lateralis and Vastus Medialis, the distribution of the MEPs is sinusoidal whereas it is V-shaped in Tibialis Anterior and linear for Gastrocnemius. The distribution of the MEPs for the targeted muscles was found to be similar among the C57BL/6 mice used in this study, thus leading to the conclusion that the organization of the MEP zones between mice of the same species is conserved. Of particular interest is the observation that the MEPs are not always found across the thickest part of the muscle (i.e., the muscle ''belly''). As a matter of fact, the thickness of Gluteus Maximus, Biceps Femoris and Gracilis is uniform across the entire muscle and therefore do not have such fleshy regions. Other muscles such as Semitendinosus have a fleshy part where the MEP regions are located but this so-called ''belly'' is not located in the center of the muscle (see Fig. 2). Previous studies have traced the hindlimb/motor neuron connectivity in various mammalian species (Hollyday, 1980; McHanwell and Biscoe, 1981; Nicolopoulos-Stournaras and Iles, 1983; Vanderhorst and Holstege, 1997; Coonan et al., 2003; Bácskai et al., 2014), however, the present work is the first study that optimized the intramuscular injection sites based on the distribution of the MEP region for each targeted hindlimb muscle.

In a series of experiments, partial portions of the MEP region for Gluteus Maximus were targeted with FG

(see Fig. 6). The rostro-caudal extent of the labeling obtained from these partial MEP injections was then compared with that resulting from injections along the full length of the MEP region, which spanned segments L3–S1. FG injections restricted to the antero-lateral half of the MEP region gave rise to labeled motor neurons occupying the rostral half of the motor neuron column that was obtained after complete MEP region injections, i.e., L3–L4. Conversely, FG injections restricted to the postero-medial half of the MEP region in the same muscle produced a column of positively labeled motor neurons spanning only the caudal half of the column of motor neurons obtained after complete MEP region injections, i.e., L5–S1. Similar results were recently obtained for the mouse Triceps Brachii muscle (Tosolini et al., 2013). Interestingly, combined labeling resulting from the injections covering the antero-lateral and postero-medial aspects of the MEP region for Gluteus Maximus resulted in a column of similar span to that produced from the injections of the complete MEP region. These results suggest the existence of a topographical relationship between the MEPs for Gluteus Maximus and the corresponding motor neurons supplying this muscle. However, more data points for Gluteus Maximus as well as for the other muscles of the mouse hindlimb will need to be generated in order to verify this *a priori* interesting set of data. Single-bolus injections into the center of the MEP region in Gluteus Maximus were also performed. Such injections yielded FG labeling in motor neurons spanning only between L4 and L6 spinal cord segments. In perspective, the short column of labeled motor neurons observed after bolus injections of FG, along with the conceivable MEP/motor neuron topographical relationship lends credence and highlights the importance of targeting the full length of a muscle's MEP region for maximum retrograde uptake. In light of these considerations, it is not surprising that the targeting of the whole extent of the MEPs gave rise to motor neurons columns that span over more spinal cord segments, on the rostro-caudal axis, than previously reported by others in the same species (McHanwell and Biscoe, 1981; Bácskai et al., 2014.

One conclusion of this work is that the mouse Gracilis muscle displays two discrete MEP bands across its muscle fibers, i.e., one near the proximal attachment and one near the distal attachment (see Fig. 2A, C). A double-innervation region across Gracilis was also reported in rats (Jarcho et al., 1952), monkeys (Kumar et al., 1998) and humans (Christensen, 1959; van Campenhout and Molenaers, 2010). Multiple MEP zones have also been reported for other skeletal muscles, in various species including humans (Bendiksen et al., 1981; Duxson and Sheard, 1995; Happak et al., 1997; Lateva et al., 2002). The presence of these double MEP zones in these aforementioned studies has been demonstrated through means of histochemical and electrophysiological techniques. In human facial muscles, for instance, four different MEP distribution patterns were present on muscle fibers: (1) single fibers innervated by one MEP, (2) single fibers innervated by two adjacent MEPs, (3) single fibers innervated by two MEPs that are further apart and (4) single fibers innervated by more than two MEPs (Happak et al., 1997). To our knowledge, however, such phenomenon has never been reported in the mouse. This observation raises an important issue regarding the innervation pattern of motor units for Gracilis. Indeed, one could ask whether these two MEP bands are innervated by separate motor neurons or, else, from collaterals of the same motor neurons. In an attempt to address this question, we targeted the two MEP regions of the Gracilis muscle with FG, either together or individually (i.e., only the proximal or only the distal MEP band). Such intramuscular injections all gave rise to columns of FG-labeled motor neurons in the same rostro-caudal compartments of the spinal cord, namely segments L1–L5. Interestingly, the cellular density of the columns of FG-positive motor neurons spanning segments L1–L5 was essentially similar, whether the intramuscular injections of FG were aimed at only one or both MEP bands. This latter result suggests that collaterals from the same motor neurons innervate both MEP bands. In a subsequent experiment, each MEP band on Gracilis was targeted with neuronal tracers of different emission/excitation wavelength, namely FG and Fluorescein. This procedure resulted in the double staining of many motor neurons, establishing that these motor neurons send a collateral to both MEP bands (see Fig. 7). Such phenomenon has also been reported before in the human larynx (Périé et al., 1997), although these results do not allow one to make any assumptions at the level of the individual muscle fibers. For instance, the collaterals of these double-labeled motor neurons could innervate the same muscle fiber twice (i.e., at the location of both the proximal and the distal MEP bands). Conversely, they could supply opposite ends on neighboring muscle fibers (Lateva et al., 2002).

Methodological considerations

In the current study, care was taken to ensure that hindlimb muscles of different functional groups were incorporated. For instance, Vastus Lateralis and Vastus Medialis are both knee extensors. Biceps Femoris is a knee flexor while Semitendinosus functions both as a knee flexor and as a hip extensor. Gracilis functions as a hindlimb adductor and Gluteus Maximus acts as a hindlimb extensor and abductor. Gastrocnemius functions as both a knee flexor and a foot dorsiflexor whereas Tibialis Anterior functions as a foot plantar flexor. In tandem with this, superficial muscles were targeted preferentially over deep muscles primarily due to their accessibility. Targeting deeper muscles would require more invasive surgery involving cutting and reflecting of superficial muscles, which could potentially lead to tracer uptake by non-targeted muscles. Effort was also taken to select muscles that are currently utilized as targets for therapy, such as Gastrocnemius and Tibialis Anterior (Mohajeri et al., 1998; Benedusi et al., 2012; Gifondorwa et al. 2012). It is our opinion that the superficial muscles of the hindlimb have greater translational relevance than the deeper ones, as they are more likely to be the target in pre-clinical trials involving somatic gene therapy.

The retrograde tracer FG has many properties that make it well suited as the neuronal tracer of choice in this study. In our hands, FG has proven to be a robust retrograde tracer that produces intense labeling of the neuronal soma and processes, therefore allowing for easy identification of motor neurons (see Fig. 4). This tracer has a prolonged life within the neurons as well as high resistance to fading (Schmued and Fallon, 1986). However, leakage has been recently reported after intramuscular injections of FG in the mouse forelimb (Bácskai et al., 2013). To avoid spurious labeling of motor neurons, the targeted muscles were routinely wiped immediately after each injection in order to remove any tracer that may have seeped out. Care was also taken to prevent leakage of the tracer into surrounding muscles by ensuring minimal disruption of the fasciae of the muscle of interest with the micropipettes. It is also worth mentioning that the fasciae enveloping the muscles were difficult to puncture even with the sharpest glass micropipettes. The resistance offered by the fasciae would have prevented the inadvertent penetration of the glass micropipettes into underlying muscles. We are therefore confident that the minute amount of tracer injected did not contaminate the muscles underlying those of interest. We also addressed this experimentally by applying FG (4 µl) to the intact fasciae covering Gluteus Maximus (n = 4). Under these conditions, no FG-labeled motor neurons were observed, a finding that is consistent with previous work in our laboratory in the mouse forelimb (Tosolini et al., 2013).

Translational relevance

Neuromuscular dysfunctions are among the most debilitating neurological conditions. In health, the muscle/motor neuron communication is made possible by the contact of the pre-synaptic terminals of motor neurons with the highly excitable post-synaptic region of the neuromuscular junction, i.e., the MEPs of a muscle. Typical phenotype associated with neuromuscular dysfunction include muscular atrophy and weakness in both upper and lower limbs which results from disrupted communication between the skeletal muscles and associated motor neurons. Mouse models are available for various neuromuscular dysfunctions such as amyotrophic lateral sclerosis (ALS), spinal muscular atrophy and Duchenne muscular dystrophy (Hsieh-Li et al., 2000; Kaspar et al., 2003; Ishiyama et al., 2004; Turner et al., 2009; Wegorzewska et al., 2009; Kimura et al., 2010; Pratt et al., 2013). These transgenic mouse models are used to explore the mechanisms of the diseases as well as for the development of treatment strategies to halt the progression of these neurological conditions. In this regard, therapeutic directions aiming to overcome such neuromuscular dysfunction phenotypes include peripheral targeting of the neuromuscular junction and the central targeting of the spinal cord motor neurons. Peripheral targeting can involve the delivery of therapeutic protein(s) to the skeletal muscles in order to maintain the integrity of the neuromuscular junction (for a review, see Krakora et al., 2012). In animal models of ALS, the delivery of GDNF to the muscle has been shown to increase the strength of the neuromuscular junction (Suzuki et al., 2008) and to delay the onset of the disease (Li et al., 2007). Intramuscular injections can also be performed to achieve central targeting of spinal cord motor neurons. Indeed, intramuscular delivery and the subsequent retrograde transport of viral vectors containing the transgene sequence for a therapeutic molecule to the corresponding motor neuron pool is an established methodology (Baumgartner and Shine, 1998; Acsadi et al., 2002; Kaspar et al., 2003; Azzouz et al., 2004: Nakajima et al., 2008; Wu et al., 2009; Uchida et al., 2012; Benkhelifa-Ziyyat et al., 2013; for a review see Federici and Boulis, 2012). Therefore, knowledge of the muscle–motor neuron topography is crucial in order to adequately analyze such potential therapies.

Previous studies have shown that the efficacy of substance absorption at the neuromuscular junction is increased with the proximity of its delivery to the motor end plate (Shaari and Sanders, 1993; Chin et al., 2005; Gracies et al. 2009; Van Campenhout and Molenaers, 2010). Indeed, MEPs are highly specialized structures on the skeletal muscle that offer direct access to the spinal cord motor neurons. Our work has clearly demonstrated that targeting the entire MEP region of a muscle results in significantly greater uptake at the neuromuscular junction and hence, better retrograde transport to the corresponding spinal cord motor neurons (Fig. 6) (see Tosolini et al., 2013). By describing (1) the details of the MEP organization on selected hindlimb muscles in the mouse and (2) the muscle/motor neuron topographical relationship, the present work will prove to be a valuable tool to explore novel treatment strategies for neuromuscular dysfunctions.

CONFLICT OF INTEREST

The authors declare that the research was conducted in the absence of any commercial or financial relationships that could be construed as a potential conflict of interest.

Acknowledgments—The authors wish to thank Mr. Andy Ho and Mr. Brian Premkumar for technical support. This work was funded by a National Health and Medical Research Centre (NHMRC) project grant and a Brain Foundation - Australia project grant to Renée Morris.

REFERENCES

Acsadi G, Anguelov RA, Yang H, Toth G, Thomas R, Jani A, Wang Y, Ianakova E, Mohammad S, Lewis RA, et al (2002) Increased survival and function of SOD1 mice after Glial Cell-derived Neurotrophic Factor gene therapy. Hum Gene Ther 13:1047–1059.

Azzouz M, Ralph GS, Storkebaum E, Walmsley LE, Mitrophanous KA, Kingsman SM, Carmeliet P, Mazarakis ND (2004) VEGF delivery with retrogradely transported lentivector prolongs survival in a mouse ALS model. Nature 429:413–417.

Baumgartner BJ, Shine HD (1998) Neuroprotection of spinal motoneurons following targeted transduction with an adenoviral vector carrying the gene for glial cell line-derived neurotrophic factor. Exp Neurol 153:102–112.

Bácskai T, Fu Y, Sengul G, Rusznák Z, Paxinos G, Watson C (2013) Musculotopic organization of the motor neurons supplying

forelimb and shoulder girdle muscles in the mouse. Brain Struct Funct 218:221–238.
Bácskai T, Rusznák Z, Paxinos G, Watson C (2014) Musculotopic organization of the motor neurons supplying the mouse hindlimb muscles: a quantitative study using Fluoro-Gold retrograde tracing. Brain Struct Funct 219:303–321.
Bendiksen FS, Dahl HA, Teig E (1981) Innervation pattern of different types of muscle fibres in the human thyroarytenoid muscle. Acta Otolaryngol 91:391–397.
Benedusi V, Martorana F, Brambilla L, Maggi A, Rossi D (2012) The peroxisome proliferator-activated receptor (PPAR) controls natural protective mechanisms against lipid peroxidation in amyotrophic lateral sclerosis. J Biol Chem 287:35899–35911.
Benkhelifa-Ziyyat S, Besse A, Roda M, Duque S, Astord S, Carcenac R, Marais T, Barkats M (2013) Intramuscular scAAV9-SMN injection mediates widespread gene delivery to the spinal cord and decreases disease severity in SMA mice. Mol Ther 21:282–290.
Chin T, Nattrass GR, Selber P, Graham HK (2005) Accuracy of intramuscular injection of botulinum toxin A in juvenile cerebral palsy – a comparison between manual needle placement and placement guided by electrical stimulation. J Pediatr Orthop 25:286–291.
Christensen E (1959) Topography of terminal motor innervation in striated muscles from stillborn infants. Am J Phys Med 38:65–78.
Coonan JR, Bartlett PF, Galea MP (2003) Role of EphA4 in defining the position of a motoneuron pool within the spinal cord. J Compd Neurol 458:98–111.
Duxson MJ, Sheard PW (1995) Formation of new myotubes occurs exclusively at the multiple innervation zones of an embryonic large muscle. Dev Dyn 204:391–405.
Federici T, Boulis NM (2012) Gene therapy for amyotrophic lateral sclerosis. Neurobiol Dis 48:236–242.
Flood DG, Reaume AG, Gruner JA, Hoffman EK, Hirsch JD, Lin Y-G, Dorfman KS, Scott RW (1999) Hindlimb motor neurons require Cu/Zn superoxide dismutase for maintenance of neuromuscular junctions. Am J Pathol 155:663–672.
Gifondorwa DJ, Jimenz-Moreno R, Hayes CD, Rouhani H, Robinson MB, Strupe JL, Caress J, Milligan C (2012) Administration of recombinant heat shock protein 70 delays peripheral muscle denervation in the SOD1(G93A) mouse model of amyotrophic lateral sclerosis. Neurol Res Int 2012:170426.
Gould TW, Oppenheim RW (2011) Motor neuron trophic factors: therapeutic use in ALS? Brain Res Rev 67:1–39.
Gracies JM, Lugassy M, Weisz DJ, Vecchio M, Flanagan S, Simpson DM (2009) Botulinum toxin dilution and endplate targeting in spasticity: a double-blind controlled study. YAPMR 90(9–16):e2.
Greene, EC (1935) Anatomy of the rat. Transactions of the American Philosophical Society. New Series, Vol. 27, pp ii-vii + ix-xi + 1–370.
Happak W, Liu J, Burggasser G, Flowers A, Gruber H, Freilinger G (1997) Human facial muscles: dimensions, motor endplate distribution, and presence of muscle fibres with multiple motor endplates. Anat Rec 249:276–284.
Henriques A, Pitzer C, Dittgen T, Klugmann M, Dupuis L, Schneider A (2011) CNS-targeted viral delivery of G-CSF in an animal model for ALS: improved efficacy and preservation of the neuromuscular unit. Mol Ther 19:284–292.
Hollyday M (1980) Organization of motor pools in the chick lumbar lateral motor column. J Compd Neurol 194:143–170.
Hsieh-Li HM, Chang JG, Jong YJ, Wu MH, Wang NM, Tsai CH, Li H (2000) A mouse model for spinal muscular atrophy. Nat Genet 24:66–70.
Ishiyama T, Okada R, Nishibe H, Mitsumoto H, Nakayama C (2004) Riluzole slows the progression of neuromuscular dysfunction in the wobbler mouse motor neuron disease. Brain Res 1019:226–236.
Jarcho LW, Eyzaguirre C, Berman B, Lilienthal JL (1952) Spread of excitation in skeletal muscle; some factors contributing to the form of the electromyogram. Am J Physiol 168:446–457.
Kanning KC, Kaplan A, Henderson CE (2010) Motor neuron diversity in development and disease. Annu Rev Neurosci 33:409–440.
Kaspar BK, Lládo J, Sherkat N, Rothstein JD, Gage FH (2003) Retrograde viral delivery of IGF-1 prolongs survival in a mouse ALS model. Science 301:839–842.
Kimura E, Li S, Gregorevic P, Fall BM, Chamberlain JS (2010) Dystrophin delivery to muscles of mdx mice using lentiviral vectors leads to myogenic progenitor targeting and stable gene expression. Mol Ther 18:206–213.
Krakora D, Macrander C, Suzuki M (2012) Neuromuscular junction protection for the potential treatment of amyotrophic lateral sclerosis. Neurol Res Int 2012:379657.
Kumar VP, Liu J, Lau HK, Pereira BP, Shen Y, Pho RW (1998) Neurovascular supply of the gracilis muscle: a study in the monkey and human. Plast Reconstr Surg 101:1854–1860.
Lateva ZC, McGill KC, Johanson ME (2002) Electrophysiological evidence of adult human skeletal muscle fibres with multiple endplates and polyneuronal innervation. J Physiol (Lond) 544:549–565.
Li W, Brakefield D, Pan Y, Hunter D, Myckatyn TM, Parsadanian A (2007) Muscle-derived but not centrally derived transgene GDNF is neuroprotective in G93A-SOD1 mouse model of ALS. Exp Neurol 203:457–471.
McHanwell S, Biscoe TJ (1981) The localization of motoneurons supplying the hindlimb muscles of the mouse. Philos Trans Royal Soc B: Biol Sci 293:477–508.
Mohajeri MH, Figlewicz DA, Bohn MC (1998) Selective loss of alpha motoneurons innervating the medial gastrocnemius muscle in a mouse model of amyotrophic lateral sclerosis. Exp Neurol 150:329–336.
Nakajima H, Uchida K, Kobayashi S, Inukai T, Yayama T, Sato R, Mwaka E, Baba H (2008) Target muscles for retrograde gene delivery to specific spinal cord segments. Neurosci Lett 435:1–6.
Ngo ST, Baumann F, Ridall PG, Pettitt AN, Henderson RD, Bellingham MC, McCombe PA (2012) The relationship between Bayesian motor unit number estimation and histological measurements of motor neurons in wild-type and SOD1(G93A) mice. Clin Neurophysiol 123:2080–2091.
Nicolopoulos-Stournaras S, Iles JF (1983) Motor neuron columns in the lumbar spinal cord of the rat. J Compd Neurol 217:75–85.
Périé S, St Guily JL, Callard P, Sebille A (1997). Innervation of adult human laryngeal muscle fibres. J Neurol Sci 149:81–86.
Pratt SJP, Shah SB, Ward CW, Inacio MP, Stains JP, Lovering RM (2013) Effects of in vivo injury on the neuromuscular junction in healthy and dystrophic muscles. J Physiol (Lond) 591:559–570.
Schmued LC, Fallon JH (1986) Fluoro-Gold: a new fluorescent retrograde axonal tracer with numerous unique properties. Brain Res 377:147–154.
Shaari CM, Sanders I (1993) Quantifying how location and dose of botulinum toxin injections affect muscle paralysis. Muscle Nerve 16:964–969.
Suzuki M, McHugh J, Tork C, Shelley B, Hayes A, Bellantuono I, Aebischer P, Svendsen CN (2008) Direct muscle delivery of GDNF with human mesenchymal stem cells improves motor neuron survival and function in a rat model of familial ALS. Mol Ther 16:2002–2010.
Tosolini AP, Morris R (2012) Spatial characterization of the motor neuron columns supplying the rat forelimb. Neuroscience 200:19–30.
Tosolini AP, Mohan R, Morris R (2013) Targeting the full length of the motor end plate regions in the mouse forelimb increases the uptake of Fluoro-Gold into corresponding spinal cord motor neurons. Front Neurol 4:1–10.
Turner BJ, Parkinson NJ, Davies KE, Talbot K (2009) Survival motor neuron deficiency enhances progression in an amyotrophic lateral sclerosis mouse model. Neurobiol Dis 34:511–517.
Uchida K, Nakajima H, Hirai T, Yayama T, Chen K, Guerrero AR, Johnson WE, Baba H (2012) The retrograde delivery of adenovirus vector carrying the gene for brain-derived neurotrophic factor protects neurons and oligodendrocytes from

apoptosis in the chronically compressed spinal cord of twy/twy mice. Spine 37:2125–2135.

Van Campenhout A, Molenaers G (2010) Localization of the motor endplate zone in human skeletal muscles of the lower limb: anatomical guidelines for injection with botulinum toxin. Dev Med Child Neurol 53:108–119.

Vanderhorst VG, Holstege G (1997) Organization of lumbosacral motoneuronal cell groups innervating hindlimb, pelvic floor, and axial muscles in the cat. J Compd Neurol 382:46–76.

Watson C, Paxinos G, Kayalioglu G, Heise C (2009) ''Atlas of the mouse spinal cord'', in spinal cord: a Christopher and Dana Reeve Foundation Text and Atlas (Watson C, Paxinos G, Kayalioglu G, eds), pp. 308–379. San Diego: Elsevier.

Wegorzewska I, Bell S, Cairns NJ, Miller TM, Baloh RH (2009) TDP-43 mutant transgenic mice develop features of ALS and frontotemporal lobar degeneration. Proc Natl Acad Sci USA 106:18809–18814.

Wu R, Wang H, Xia X, Zhou H, Liu C, Castro M, Xu Z (2009) Nerve injection of viral vectors efficiently transfers transgenes into motor neurons and delivers RNAi therapy against ALS. Antioxid Redox Signal 11:1523–1534.

(Accepted 21 May 2014)
(Available online 2 June 2014)